

RESEARCH ARTICLE

10.1002/2015JA021417

Key Points:

- We show how to track separators in 3-D models with or without magnetic nulls
- Reconnection occurs all along the separator
- FTE results in local and global reconnection rate decrease

Correspondence to:

A. Glocer,
alex.glocer-1@nasa.gov

Citation:

Glocer, A., J. Dorelli, G. Toth, C. M. Komar, and P. A. Cassak (2016), Separator reconnection at the magnetopause for predominantly northward and southward IMF: Techniques and results, *J. Geophys. Res. Space Physics*, 121, 140–156, doi:10.1002/2015JA021417.

Received 30 APR 2015

Accepted 16 OCT 2015

Accepted article online 20 OCT 2015

Published online 6 JAN 2016

Separator reconnection at the magnetopause for predominantly northward and southward IMF: Techniques and results

A. Glocer¹, J. Dorelli¹, G. Toth², C. M. Komar³, and P. A. Cassak³

¹NASA/Goddard Space Flight Center, Greenbelt, Maryland, USA, ²Department of Atmospheric, Oceanic, and Space Sciences, University of Michigan, Ann Arbor, Michigan, USA, ³Department of Physics and Astronomy, West Virginia University, Morgantown, West Virginia, USA

Abstract In this work, we demonstrate how to track magnetic separators in three-dimensional simulated magnetic fields with or without magnetic nulls, apply these techniques to enhance our understanding of reconnection at the magnetopause. We present three methods for locating magnetic separators and apply them to 3-D resistive MHD simulations of the Earth's magnetosphere using the Block-Adaptive-Tree Solar-wind Roe-type Upwind Scheme code. The techniques for finding separators and determining the reconnection rate are insensitive to interplanetary magnetic field (IMF) clock angle and can in principle be applied to any magnetospheric model. Moreover, the techniques have a number of advantages over prior separator finding techniques applied to the magnetosphere. The present work examines cases of high and low resistivity for two clock angles. We go beyond previous work examine the separator during Flux Transfer Events (FTEs). Our analysis of reconnection on the magnetopause yields a number of interesting conclusions: Reconnection occurs all along the separator even during predominately northward IMF cases. Multiple separators form in low-resistivity conditions, and in the region of an FTE the separator splits into distinct branches. Moreover, the local contribution to the reconnection rate, as determined by the local parallel electric field, drops in the vicinity of the FTE with respect to the value when there are none.

1. Introduction

Magnetic reconnection plays a major role in space plasma physics. Indeed, the picture of *Dungey* [1961], in which the solar wind couples to the magnetosphere via reconnection, is the accepted paradigm of solar wind-magnetosphere coupling. Much of our thinking about reconnection is in a two-dimensional context of a local process of oppositely directed field lines forming an X line configuration. However, reconnection at the magnetopause is a fundamentally three-dimensional process. In three-dimensions, the definition of magnetic reconnection has been the subject of considerable debate [Vasyliunas, 1975; Schindler and Hesse, 1988; Hesse and Schindler, 1988; Dorelli et al., 2007] and ideas differ on how to locate regions where reconnection is occurring.

In this paper we focus on the concept of separator reconnection [Priest and Forbes, 2000]. Qualitatively, a magnetic separator can be thought of as the 3-D analog of the 2-D X line. Separatrix surfaces divide regions of magnetic field into topologically distinct regions. The magnetic separator is defined by the intersection of separatrix surfaces and thus represents the junction of four topologically distinct flux regions. In the context of the magnetopause, the separator separates closed field lines whose foot points are both mapped to the Earth, open field lines that have one foot point mapped to the Earth and the end mapped to the solar wind, and solar wind field lines that have both ends in the solar wind. Cowley [1973] qualitatively described separators at the magnetopause in the context of a simple vacuum superposition topology obtained by superimposing a uniform magnetic field on a magnetic dipole and using it to present the idea that the potential drop along the separator defines the reconnection rate. Conceptually, a separator bounds the region of closed magnetic flux, and so the line integral of the electric field parallel to the separator gives the rate of change of closed magnetic flux. Since the rate of change of closed flux must match the rate of change of open flux, the potential drop along the separator gives the rate of open flux production, a general way to define reconnection. For further discussion regarding separator reconnection in general, we refer readers to the work of Lau and Finn [1990] and the textbook by Priest and Forbes [2000].

Locating magnetic separators is extremely challenging. As the collection of points representing the junction of four topologies, a point on the separator cannot possess any of the four topologies. Therefore, a separator on the magnetopause must be a magnetic field line that closes on itself. We illustrate the difficulty in identifying this unique separator line out of the infinite number of possible lines in the following scenario. Assume that you have managed to identify a single point on the separator; in principal, additional points can be found by tracing the field line through that point. However, no matter how accurate a field line tracing algorithm is, there is always numerical error that puts the next point identified ever so slightly off the separator. From that point on all of the points identified will have one of the four topologies rather than a loop which the separator must have. Despite these challenges a few methods have been proposed to locate separators.

The simplest method that can determine the approximate location of the separator traces many field lines in an attempt to locate the separator. The numerical considerations described above imply that this technique can never be successful, but it is possible to find a line that approximates the location of the separator. *Dorelli et al.* [2007] is an example of such an approach to find a separator field line. They trace field lines along the Sun-Earth line and select the one that gets close to the magnetic nulls and thus approximates the separator.

Another class of methods takes advantage of the fact that separators often connect nulls. These methods start by first locating the nulls. In the case of *Haynes and Parnell* [2010], a pair of rings of points is created around one of the nulls, field lines are then traced a short distance. Should the distance expand beyond a given tolerance additional points are added. This procedure continues until another null is encountered. In a final “trace-back” step, the points on each ring are traced backward from the recently encountered null to the starting null which yields the separator. *Komar et al.* [2013] also start by finding nulls but then find additional points on the separator by sampling the topology on a hemisphere surrounding a given null and locating intersections on the surface of that hemisphere. The process is repeated until another null is encountered. These two methods have the advantage that they do not involve finding the separator by the brute force, and ultimately unsuccessful, approach tracing of many lines, but they rely on initially locating nulls. However, this method only locates separators that join magnetic nulls and so cannot be used in situations where there are no nulls. Separators in the absence of nulls are known to exist in tokamaks [e.g., *Boozer*, 2005] and, to our knowledge, are not precluded in the magnetosphere either.

Yet another approach is to constrain the probable location of the separator by highly sampling the region where the separator is expected to exist; the studies of *Laitinen et al.* [2006, 2007] take this approach. In their method, the separator is found by first identifying where you expect the separator to be and then highly sampling the topology in that region. That region is divided up into small volumes, and any volume that contains sampled points with all four topologies is considered to be a point on the separator. This approach is successful in locating junctions of four topologies but has two significant drawbacks. First, the volume of interest must be extremely highly sampled resulting in a large amount of work to trace field lines. Second, the volume must be preselected to avoid having to densely sample the entire simulation domain.

The above methods for locating separators primarily focus on approaches applied to the magnetosphere. There is also a very rich literature of separator locating techniques applied in the solar context including: the midplane method [*Longcope*, 1996], the progressive interpolation method [*Close et al.*, 2004], the simulated annealing method [*Beveridge*, 2006], and the method combining a modified progressive interpolation method with Q maps [*Titov et al.*, 2012]. This last method has the advantage that it does not rely on the presence of nulls in the configuration. We do not go further into these methods here but instead refer the interested reader to the above publications.

In this paper we describe new approaches to locating magnetic separators at Earth’s magnetopause (section 2). These new approaches are able to find separators in the absence of nulls and can handle situations in which there exist multiple separators. Moreover, some of the new methods introduced are easily parallelized making them able to locate separators quickly. These attributes represent an advance over previous separator finding techniques applied to the magnetosphere. We then present applications of those methods as applied to resistive MHD simulations (section 3). The ability to reliably and accurately locate separators allows for exciting new studies of 3-D reconnection. Indeed, a number of intriguing new results are uncovered. We discuss the implications of our results for understanding reconnection on the dayside magnetopause (section 4).

2. Three Methods for Finding Magnetic Separators

We present three methods for finding magnetic separators in numerical simulations. The algorithm for each method is described, as are details relating to implementation and performance. The advantages and drawbacks of each method are also discussed.

Our first method for finding magnetic separators, henceforth referred to as method 1, is to find the magnetic separatrix surfaces defining the open-closed boundary and the open solar wind boundary and then finding their points of intersection. This approach is very straightforward in concept. We start by locating both surfaces by stepping radially outward from the Earth until we see a topology change from closed to open. That point is retained as a member of the set defining our open-closed separatrix surface. We then continue stepping out radially until we find where the topology changes from open to solar wind and save that point as a member of the set of points defining our open solar wind separatrix surface. Repeating this for many points allows us to highly sample both separatrix surfaces. We then evaluate the distance between the points on the two separatrix surfaces. Whenever the points are within some tolerance (in our case 1/100 of a grid cell), we assume those points represent a location where the surfaces intersect, and this point lies on the separator.

The concept of locating the separatrix surfaces in method 1 is easier to explain, as we do above, using the approach of radial stepping outward and looking for changes in the magnetic topology. In practice, we actually apply a bisection approach to finding each of separatrix surfaces. The bisection method involves sampling the magnetic topology at three points, one close to the planet, one in the solar wind, and one in the middle of the other points. Since we know that the open-closed boundary, for instance, must be between points with open and closed topologies, we can identify which two of the three initial points bound the interval containing a point on the open-closed boundary. We then choose a point in the middle of the identified interval and repeat. Our point on the separatrix surface is located once the size of the interval shrinks below some tolerance. This bisection approach to finding points on the separatrix surface is much more computationally efficient than simple radial stepping. In general, it is possible that the surfaces may intersect the radial line multiple times. In practice this may not often happen, but the algorithm is either limited to finding a single intersection, or the search has to revert to the more computationally expensive and exhaustive radial stepping search.

Our second method for finding magnetic separators, henceforth referred to as method 2, is an improved version of the technique introduced by *Komar et al.* [2013]. The steps in this method are summarized in Figure 1. We start by locating all the magnetic nulls in the simulation using the algorithm of *Greene* [1988] and labeling the nulls as positive (type A) and negative (type B) based on whether the field lines are directed into or out of the nulls according to the convention of *Cowley* [1973]. We then select a positive null and draw a sphere of some small radius (typically $2 R_E$) around it. The magnetic separator must pass through the null and we can locate where the separator pierces the sphere by finding the intersection of four topologies on the surface of the sphere. The points at those intersections are retained as belonging to the set of points defining the magnetic separator. We then find the next points along the separator by drawing spheres around the recently identified points and finding the intersections of four topologies on those spheres. This process repeats itself until a corresponding negative null is reached.

Our implementation of method 2 is similar in approach to the technique of *Komar et al.* [2013] but differs in two key ways. First, the separator is traced in both directions allowing the separator to be followed across the dayside magnetopause and through the magnetotail. Second, and more importantly, a highly accurate and efficient technique is implemented for finding the intersection of four magnetic topologies on the surface of a sphere. Our technique can find an arbitrary number of intersections to an arbitrary accuracy without having to do an exhaustive number of field line traces to cover the entire surface.

Figure 2 illustrates the algorithm for accurately and efficiently locating intersections of four topologies. Each panel in the figure shows the surface of the sphere spread out on a plane; the horizontal axis is ϕ , the azimuthal angle, and the vertical axis is θ , the polar angle. The color represents the magnetic topology at each point on the sphere's surface. The topology is shown for illustration only as the topology everywhere on the surface is not sampled by this algorithm. Our first step is to discretize the surface into some number of rectangles; Figure 2b shows the simplest choice in which the surface is divided into four quadrants. The topology is sampled along the edges of each rectangle. Any rectangle that has four topologies present on its boundary potentially contains an intersection; in Figure 2b this corresponds rectangles 1, 3, and 4. Those rectangles are

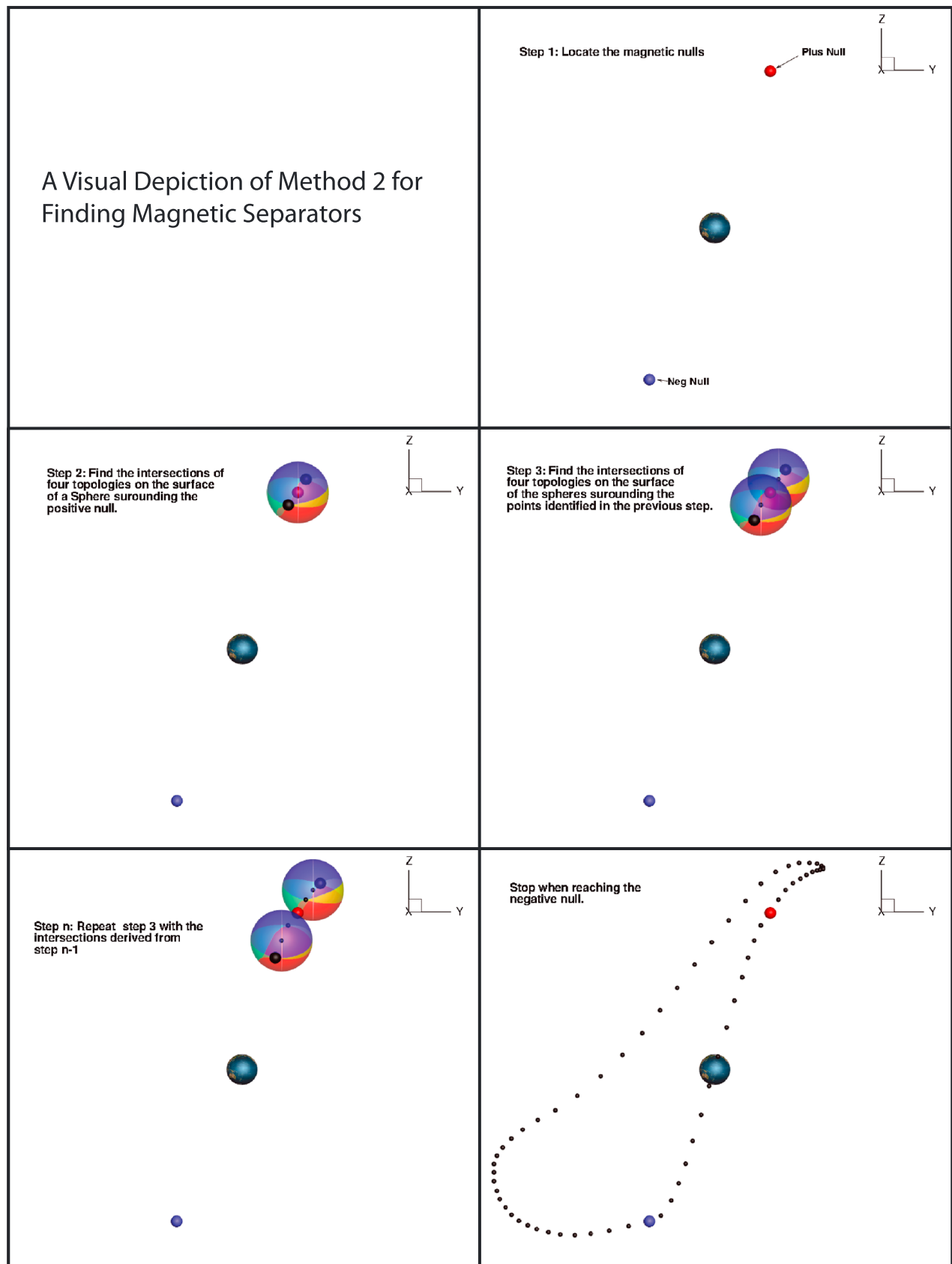


Figure 1. An illustration of method 2 for finding magnetic separators.

A General Method For Finding Points of Intersecting Topologies

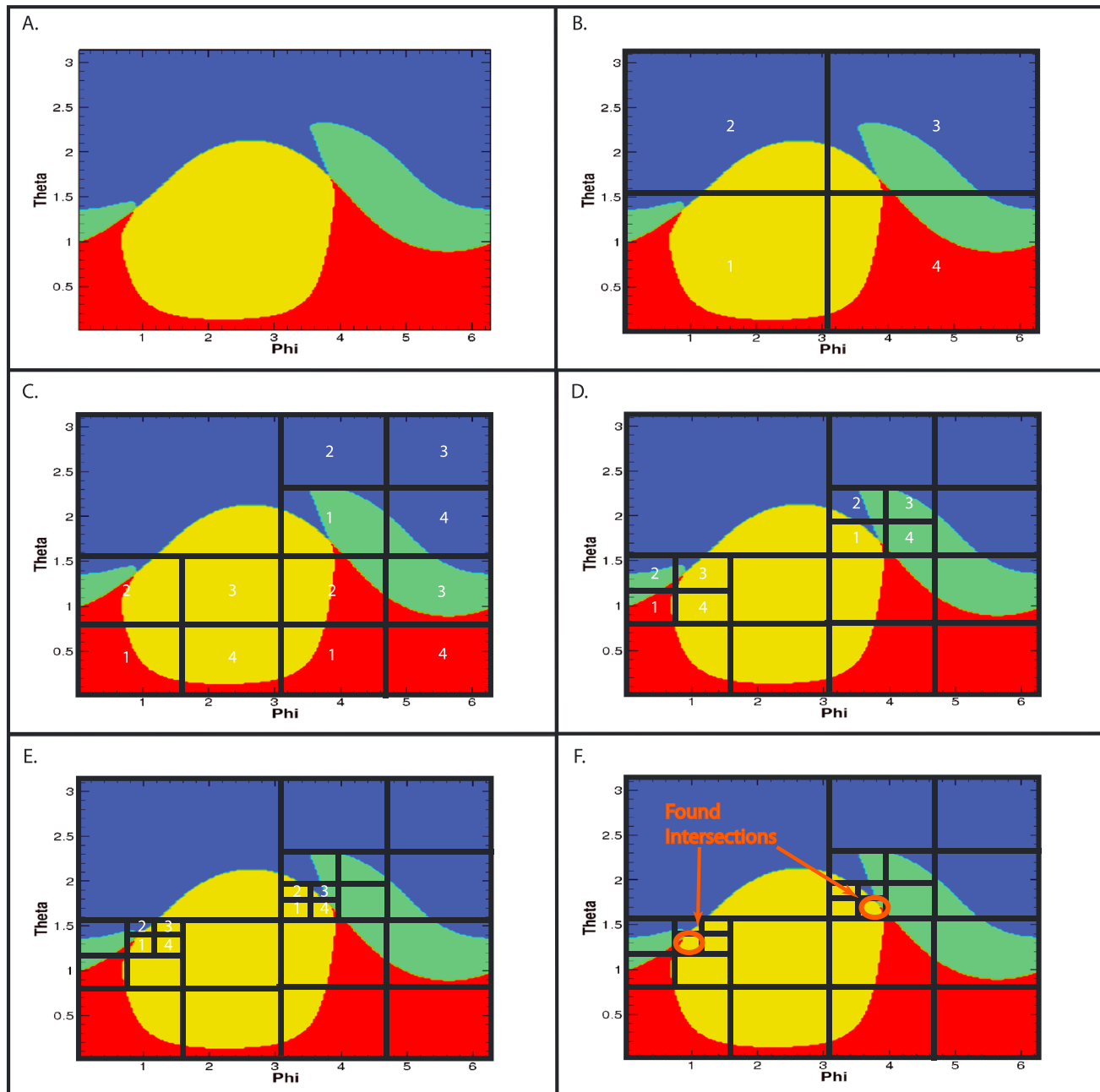


Figure 2. A schematic demonstration of a general method for finding points of intersecting magnetic topologies. (a) A plane with four colors illustrating the four topologies on that plane. Our method subdivides the plane and samples the topology along the boundary of each region. Any region that has four topologies on the boundary has the potential to contain an intersection, and that region is subdivided. (b–e) The progression. Once a region potentially containing an intersection reaches a minimum size, it is assumed that (f) actual intersection was found.

subdivided (see Figure 2c), and the topologies are sampled on the boundaries of the new rectangles. Rectangles with four topologies present on the boundary are subdivided again (see Figure 2d). Note that the false detection of rectangle 4 in Figure 2b as potentially containing an intersection is automatically corrected upon further subdivision. This process continues until the rectangle size drops below some predefined tolerance. At that point the intersections are assumed to be found.

This technique for finding intersections has a number of advantages. It does not presuppose how many intersections may be present, thus allowing for the possibility that the separator may split or that multiple

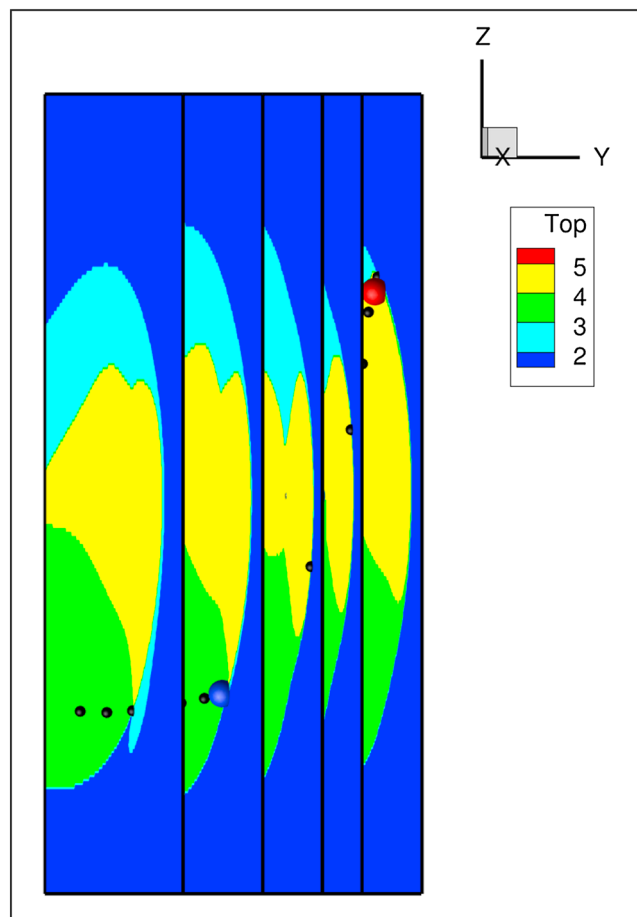


Figure 3. An illustration of method 3 for finding separators. A series of planes, in this case all parallel to the $y = 0$ plane, cut through our simulation domain. The planes are seen from a vantage point slightly offset from the Sun-Earth line. The color bar corresponds to magnetic topology and is shown for illustrative purposes. The black dots show the intersection points of four topologies found by applying our intersection-finding algorithm to a number of planes. These black dots are points along the magnetic separator. Note that more planes were used in finding the black dots than are shown here.

Methods 1 and 3 have the advantage that they are embarrassingly parallel (meaning that the method can be parallelized simply with no communication between processes) and do not require finding magnetic nulls. The ability of the methods to find separators in the absence of nulls is an advantage over most previously published methods as well, with the exception of the approach of *Titov et al.* [2012]. With method 1, we decompose the domain over which we locate the separatrix surfaces and distribute the work across processors. In method 3, we distribute the planes in which we are searching for intersections across processors; further parallelization of method 3 is possible by domain decomposition of the planes themselves. Both methods are implemented with the Message Passing Interface and, with suitable computational resources, can locate magnetic separators in a simulation fairly quickly. The ability to accurately and quickly find the separators is an advantage as compared to prior methods that also require tracing field lines to obtain topology information. We note, however, that an efficiency comparison to methods for finding the separator that rely only on local magnetic field information has not been conducted.

3. Application to Simulations Earth's Magnetosphere

We apply the magnetic separator calculation methods detailed in the previous section to resistive MHD simulations of the Earth's dayside magnetopause. Two values of uniform resistivity (η), a high resistivity

separators may be present. The intersections can be found to an arbitrary accuracy by reducing the predefined tolerance. The topology does not need to be exhaustively sampled on the surface, instead we successively subdivide the surface only sampling the topology on the edges of the rectangles. Finally, the algorithm is applicable not only to finding intersections of four topologies on a sphere but also to finding the intersections on any arbitrary surface in the simulations. This last advantage gives rise to our third method for finding magnetic separators.

Our third method for finding magnetic separators, henceforth referred to as method 3, takes advantages of the fact that the method for finding intersections works for any arbitrary plane in the simulation. Therefore, we can simply choose a series of planes slicing through the simulation and locate intersections of four magnetic topologies on those planes. Figure 3 illustrates how this method works. In this figure, a number of planes parallel to $y = 0$ (GSM) are sliced through the simulation output. The topology is shown for illustration purposes in color. The black dots represent intersections of four topologies found using our intersection-finding algorithm. The red and blue dots represent the magnetic nulls.

As we will demonstrate in the next section, each of these methods produce the same results when applied to find separators in the Earth's magnetosphere.

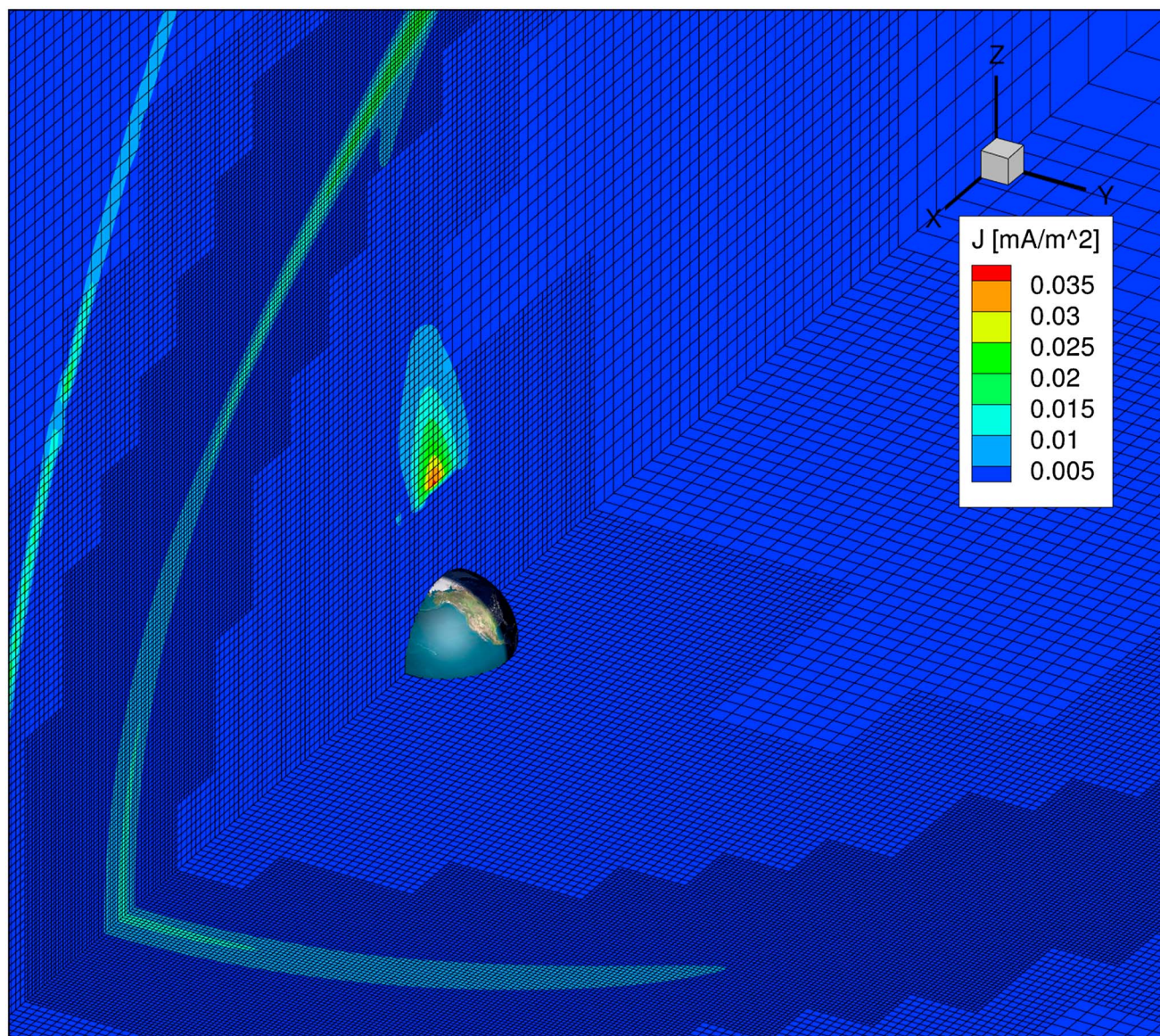


Figure 4. In all of our simulations, we choose a grid tailored for dayside magnetopause studies. Our grid uniformly resolves the dayside magnetopause with a resolution of $1/16 R_E$.

($\eta = 6 \times 10^{10} \text{ m}^2/\text{s}$) and a low-resistivity ($\eta = 2.125 \times 10^9 \text{ m}^2/\text{s}$), are used to examine how the separator depends on resistivity magnitude. These two values of resistivity were chosen so that we would have a thick stable current sheets with no Flux Transfer Events (FTEs) for high η and thin current sheets with FTEs and other instabilities for low η . We also consider two values of interplanetary magnetic field (IMF) clock angles, 135° and 45° , so that we have predominantly southward and northward cases to demonstrate the applicability of our methods to arbitrary clock angles. Strong solar wind driving is used with a magnetic field magnitude of 20 nT, density of 20 cm^{-3} , and velocity of 200 km/s; such strong driving conditions compress the magnetosphere and allow us to expend fewer computational resources to obtain high resolution of the magnetopause.

This study makes use of the Block-Adaptive-Tree Solar wind Roe-type Upwind Scheme, or BATS-R-US, code to represent the global magnetosphere. While BATS-R-US is a multiphysics code capable of solving a variety of problems [e.g., Gombosi et al., 2001; Tóth et al., 2008; Glocer et al., 2009b, 2009a], in this study we focus only on a simple configuration of resistive MHD with an ionospheric solver that has a uniform conductance of 5S specified over the entire sphere; dipole tilt and corotation are also neglected to remove potential physical

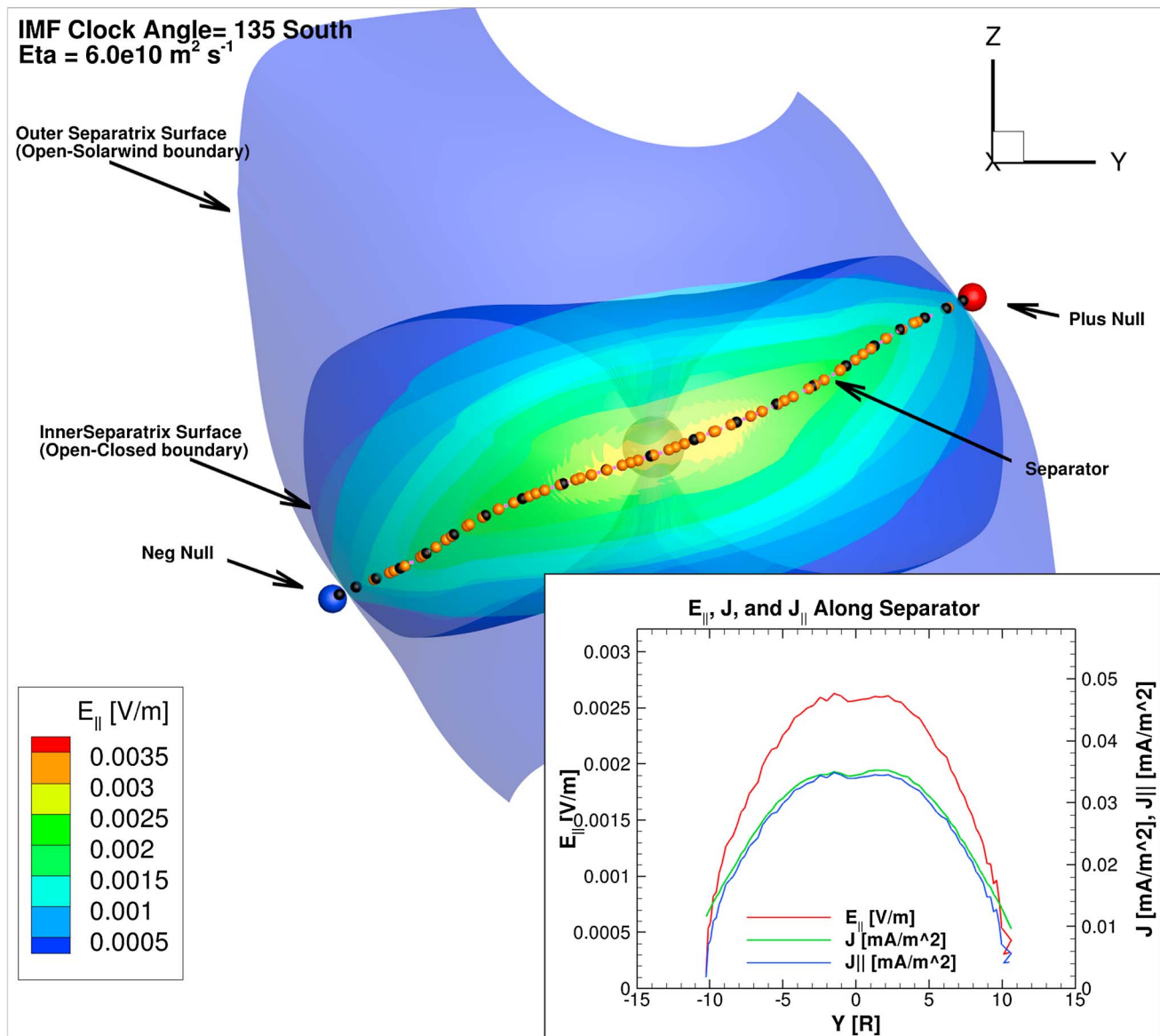


Figure 5. A comparison of our three methods for locating separators for case with a solar wind clock angle of 135° southward and a large value of resistivity (η). The vantage point is looking at the Earth from the sunward direction. The magnetic null points, separatrix surfaces (colored by E_{\parallel}), and magnetic separator are labeled. The separator found using method 1 is shown with pink dots, using method 2 is shown in black dots, and using method 3 is shown with orange dots. The inset line plot shows E_{\parallel} , J and J_{\parallel} along the separator on the dayside.

sources of asymmetry. The effect on the magnetic separator due to the effect of the ring current, ionospheric outflows, and other important features of the space environment is left to future studies.

Our simulation domain extends from $32 R_E$ upstream to $224 R_E$ downstream of the planet and $64 R_E$ to the sides. The inner boundary is a sphere of radius $2.5 R_E$ centered on the Earth. As we use a Cartesian grid with cubic cells that spherical inner boundary is necessarily approximated by defining cells external to the sphere be computational cells. The cells inside the sphere are not used in the computation. Boundary conditions are applied on the faces of the computational cells that are surrounding the spherical boundary and are adjacent to a cell inside the sphere. The grid is specifically adapted to provide a uniform resolution of $1/16 R_E$ along a thick region surrounding the dayside magnetopause. In the inner magnetosphere, the grid is $1/8 R_E$ and $1/4 R_E$ in the near-Earth tail and one half of an R_E farther away. Figure 4 shows the grid in $y = 0$ and $z = 0$ plane cuts. Such a grid ensures that we have uniform high resolution everywhere on the dayside magnetopause with multiple points across the current sheet (approximately 10) without presupposing exactly

where the magnetopause will be located. The grid resolution elsewhere is also reasonable. Our simulation domain consists of 22 million computational cells.

Figure 5 presents a comparison of our three methods for locating separators for a case with an IMF clock angle of 135° and a large value of resistivity. The vantage point is looking at the Earth from the sunward direction, and the magnetic null points, separatrix surfaces, and magnetic separator are labeled. Each method for finding the separator has a different color dot (pink, black, and orange), and they all lay on top of each other demonstrating that all methods give the same result. An inset figure shows the component of the electric field parallel to the local magnetic field (E_{\parallel}), the magnitude of the current density (J), and the component of the current density parallel to the local magnetic field (J_{\parallel}) along the separator on the dayside. The color contour on the separatrix surfaces represent the value of E_{\parallel} .

There are several interesting conclusions to draw from Figure 5. First of all, the magnetic separator on the dayside magnetopause runs along the ridge of maximum E_{\parallel} on the separatrix surfaces. The total current density and parallel current density are almost identical along the separator indicating that this line is force free and that the current sheet is organizing along the magnetic separator. E_{\parallel} is maximum in the vicinity of the subsolar point and drops toward the flanks. Therefore, we conclude that the maximum production of open flux occurs near the subsolar point on the separator for high η and southward IMF.

Figure 6 has the same format as Figure 5 except that we are now considering a simulation with a 45° IMF clock angle. As with the 135° clock angle case, a single separator connecting two magnetic nulls is found; all three methods agree and give the same result. As a demonstration that the separator makes a complete loop across the magnetopause and through the magnetotail, we allow method 2 to continue tracing the separator all the way around the planet. The total current density and parallel current density are identical in the vicinity of the subsolar point, indicating the line is force free in this region; however, the total and parallel currents diverge as we approach the nulls in the cusps. Interestingly, the maximum E_{\parallel} along the separator is near the subsolar region, not in the cusp. Therefore, open flux production is happening primarily at the subsolar region even when the IMF has a significant northward component. This result is consistent with earlier results by *Dorelli et al.* [2007] who also find that reconnection maximizes at the subsolar point for northward IMF and *Parnell et al.* [2010] who demonstrate that reconnection occurs at all points along the separator. Nevertheless, it is an important point not well known in the context of reconnection on the magnetopause.

The cases just presented were all for high-resistivity cases which resulted in magnetospheres with only two nulls, a single separator, smooth separatrix surfaces, thick current sheets, and no physical or topological instabilities. Now, we turn to the low-resistivity case. Figure 7 follows the same format as its high η counterpart (Figure 5). Only methods 1 and 3 are used for the low-resistivity case. Some differences are immediately obvious. For instance, several nulls are identified instead of only two magnetic nulls. Also, the separatrix surface are much less smooth owing to the many FTEs appearing during the simulations. As best we can determine, the sharper ripples in the surface are due to interpolation artifacts in the plotting. For the purposes of this paper, we loosely define an FTE as a twisted up magnetic flux rope forming on the magnetopause. We choose a time between FTEs to examine, approximately 1 h into the simulation. A clear separator is identified crossing the dayside magnetopause. The current sheet is aligned with the separator, as is the maximum electric field along the separator. Interestingly, there appear to be a number of other separators branching from the main separator on the right of the figure. It is not clear to us the origin of these additional separators are. However, we speculate that they are connected somehow with the disturbed state of the magnetopause with multiple FTEs forming every few minutes. We further note that there are a handful of stray points not on the main separator. It is not clear if these stray points represent the remnants of a prior FTE moving off or are simply spurious solutions to our algorithm.

Approximately 5 min before the time shown in Figure 7, an FTE of significant size forms at the subsolar magnetopause. Figure 8 demonstrates an application, our separator technique (method 3), to the case with an FTE present. The inset on the lower right of the plot shows a portion of the $y = 0$ plane that cuts through the middle of the FTE; the color contour represents pressure, and the white lines are the magnetic field stream traces using the B_x and B_z components. This inset is a typical visualization of an FTE from a global magnetosphere simulation. We see that there are two x points bounding the FTE and an o point in the middle of the FTE. That picture, however, is a deceiving construct of trying to analyze an inherently three-dimensional structure in a two-dimensional paradigm. Our separator finding techniques are able to trace all the branches of the FTE to very high accuracy. We find that there are three distinct branches of the separator. Moreover, what appear

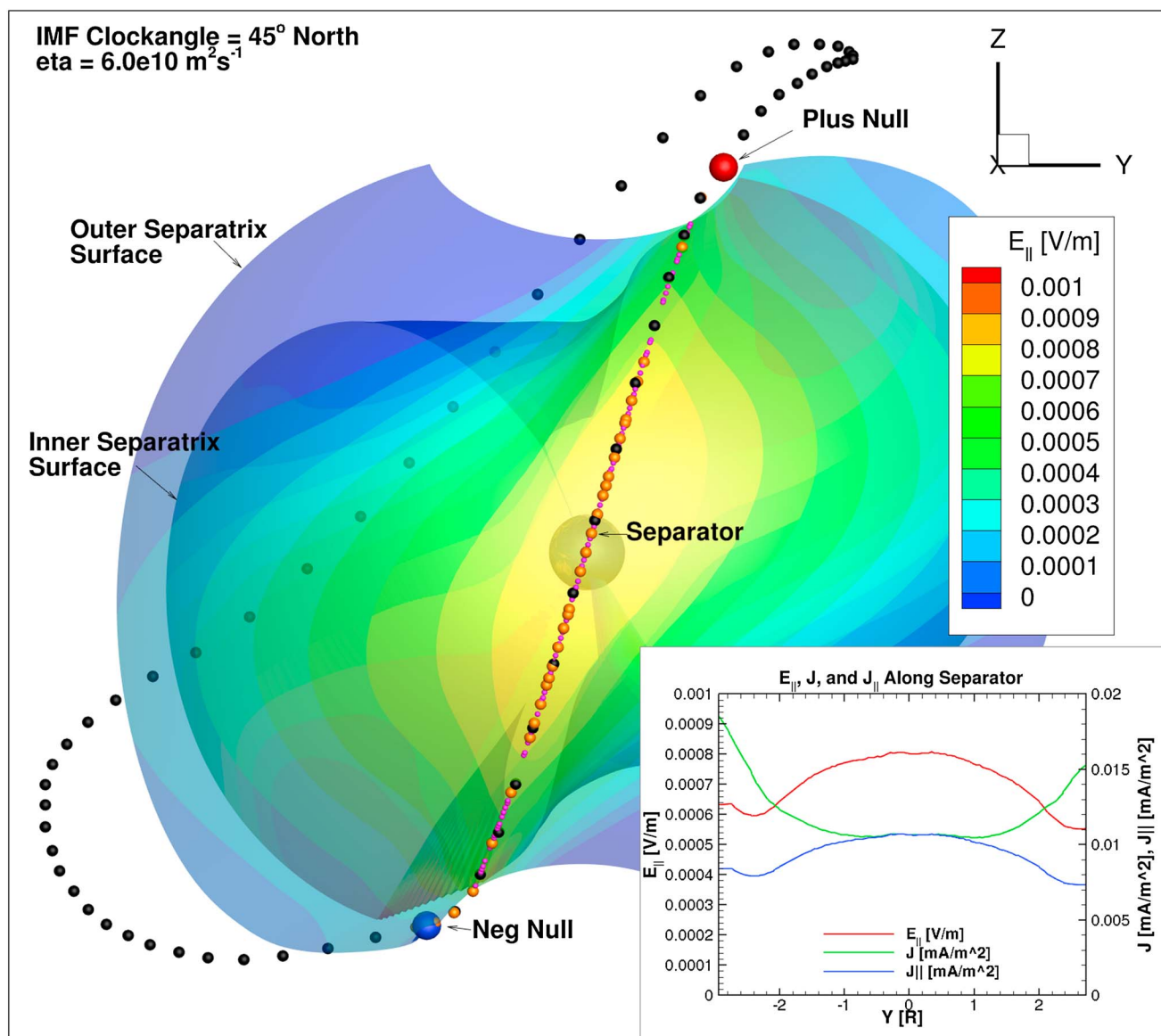


Figure 6. A comparison of our three methods for locating separators for case with a solar wind clock angle of 45° northward and a large value of resistivity (η). The vantage point is looking at the Earth from the sunward direction. The magnetic null points, separatrix surfaces, and magnetic separator are labeled. The separator found using method 1 is shown with pink dots, using method 2 is shown in black dots, and using method 3 is shown with orange dots. Methods 1 and 3 were only used on the dayside, but we continued method 2 all the way around the Earth as a demonstration that we can follow the separator into the magnetotail as well. The inset line plot shows E_{\parallel} , J , and J_{\parallel} along the separator on the dayside.

to be o-type structures in the 2-D projection are not loops in 3-D; only x-type structures represented by the separators are present in the 3-D analysis of the FTE. Furthermore, we analyze the electric field present on the separators during this time that the FTE is forming (see the lower left inset of the figure) and find that the parallel electric field actually drops in the presence of the FTE. The inset shows a scatterplot from all identified separator points, and the largest localized drop seen corresponds to the top two separators while the bottom separator has smaller drops elsewhere. Interestingly, E_{\parallel} is distributed differently along each of the separators. Since the integral of the parallel electric field along a separator is the measure of the open flux production, the presence of an FTE actually results in a modest decrease in the global reconnection rate. Locally, the decrease in E_{\parallel} is on the order of approximately 25%. Since the FTE only covers at most 25% of the dayside separator, the expected global decrease of the reconnection rate is on the order of 6%. Actually, integrating E_{\parallel} along the separator during an FTE yields a decrease of 4% in the reconnection rate compared to the time with no FTE, a value comparable to our estimate. The local electric field decrease is easily understood if the FTE is the result

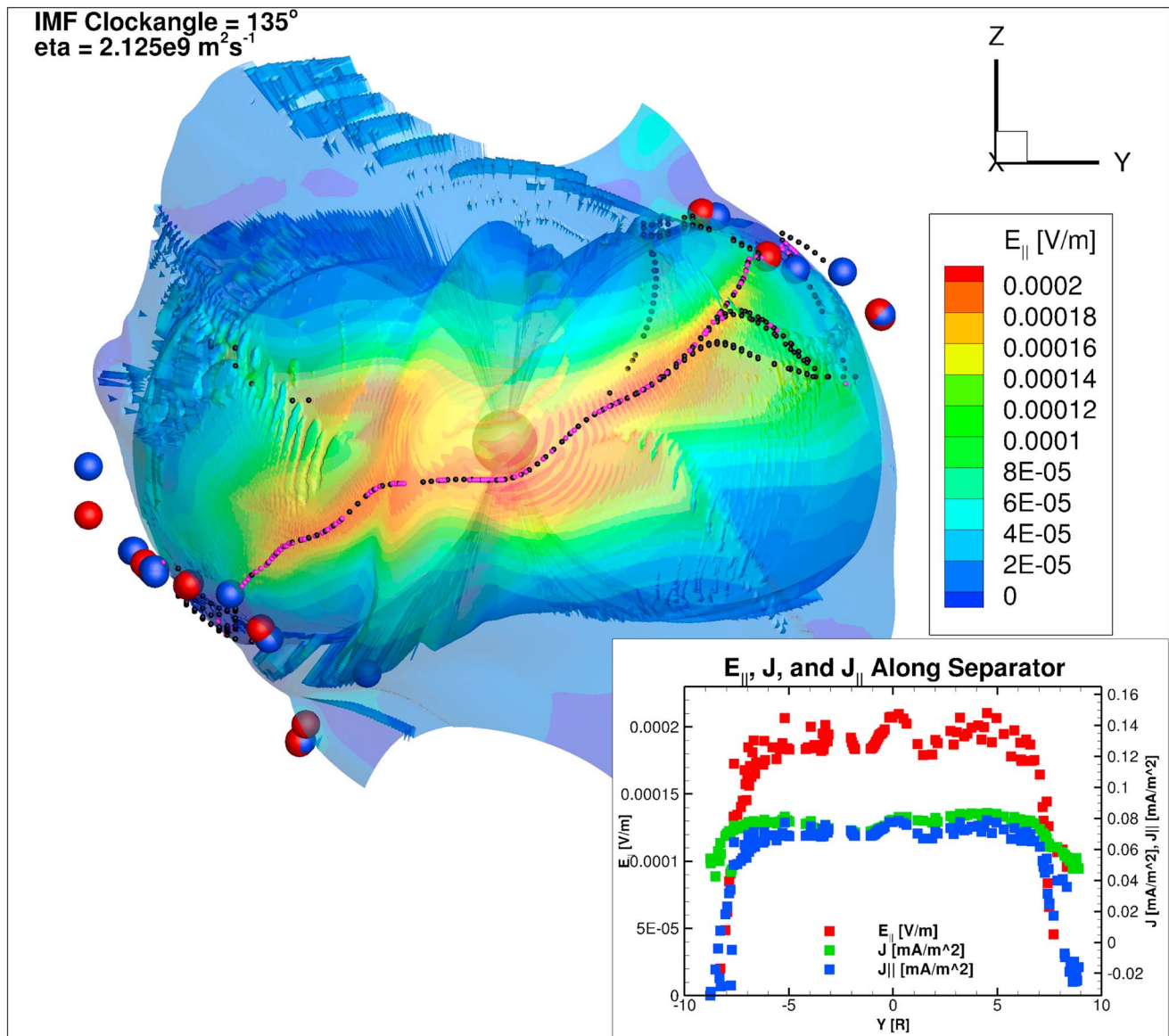


Figure 7. We use method 1 (pink dots) and method 3 (black dots) to calculate magnetic separators for a low η case when the IMF clock angle is 135° southward. This is a time in the simulation between FTE formation. Note that multiple nulls are found at the dawn and dusk flanks, and the separatrix surfaces are clearly disturbed by regular FTE formation. Nevertheless, a separator can still be found.

of a current-driven instability, as appears to be the case in our simulation. Effectively, the FTE formation coincides with a breakup of the current sheet and hence a decrease in the current density and a commensurate reduction in the parallel electric field as calculated by ηJ_{\parallel} . It is interesting to note that in 2-D the central o point is not a reconnection site, and only the two x points are reconnection sites; in 3-D, however, reconnection is occurring along each of the three separators.

Figure 9 further illustrates the differences between the 3-D FTE picture and the 2-D picture. The figure presents the separator and nulls from the previous plot, together with characteristic field lines of the FTE in grey, as well as lines chosen near each portion of the separator. Field lines near the lower branch of the separator are in red, middle branch in green, and upper branch in orange. Blue lines are field lines near the regions before the separator branches. Note that these lines are shown for illustration purposes only as there is no true characteristic line near a separator; any two points near a separator may have different topology, and field lines traced from those starting points could have very different shape. The figure also presents cut planes through the FTE showing the characteristic pressure bulge that follows the twisted up flux. It is immediately

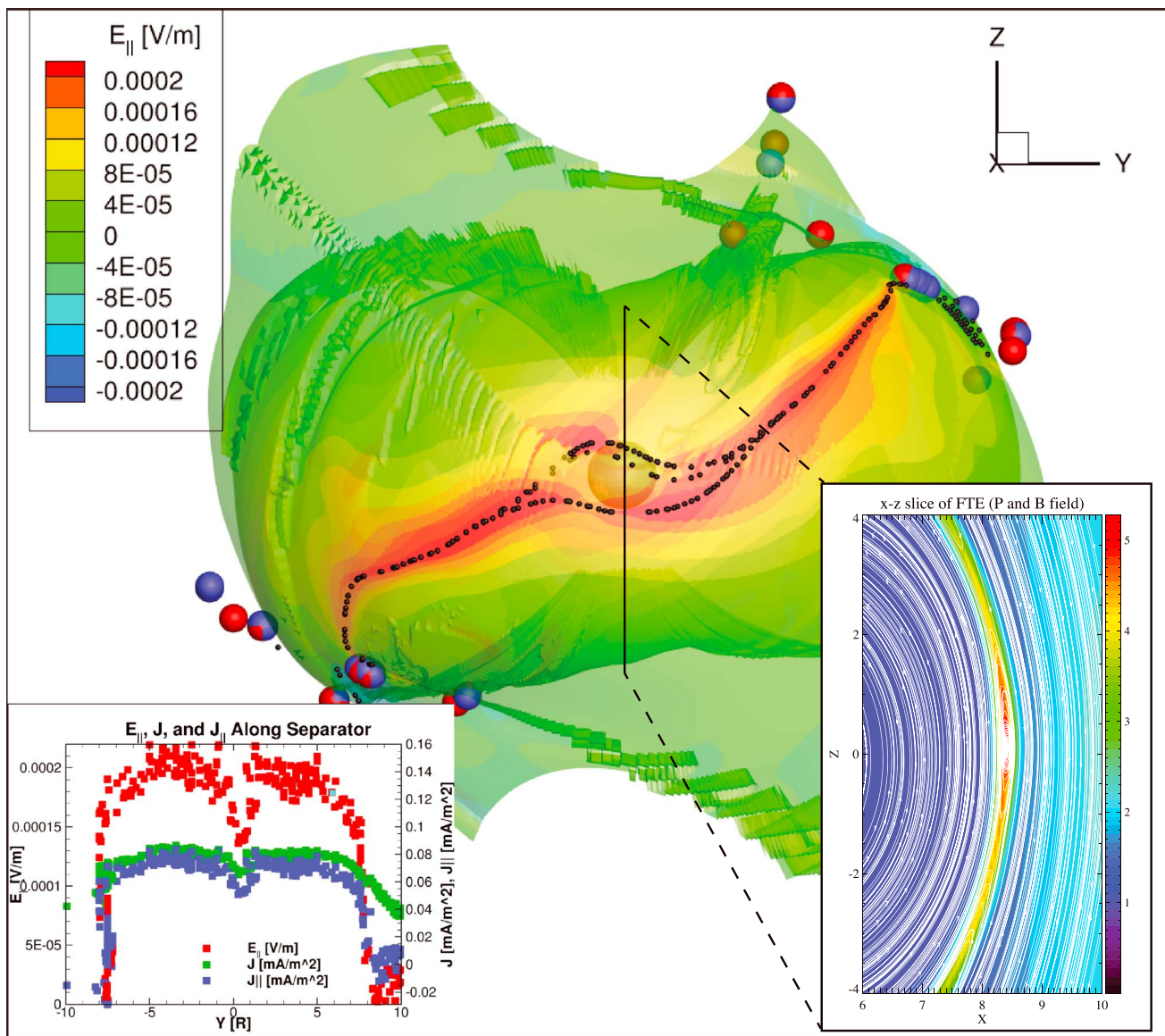


Figure 8. The magnetic separators, nulls, and separatrix surfaces are shown for the low η case when the IMF clock angle is 135° southward during FTE formation. An inset showing a slice through the FTE at the subsolar point is also shown. Note that there are now three separators in the region of the FTE, and the parallel electric field drops in this region.

apparent that the flux rope does not follow the separator, but where the flux rope intersects the separator is where the branching becomes evident. As the pressure bulge associated with the FTE is also associated with a disruption of the current sheet at the same location, the $E_{||}$ must also drop in regions where the FTE intersects the separators. It is moreover striking how much the full 3-D picture differs from the 2-D projection shown as an inset in Figure 8. The juxtaposition of these two pictures further reinforces the potential pitfalls when interpreting 3-D reconnection with a 2-D paradigm. Further detailed studies on the 3-D evolution of FTEs including their time history and interaction with the separator are left to future studies.

Figure 10 presents the low magnetic resistivity case for the 45° clock angle simulation. The format is exactly the same as for the high-resistivity case (Figure 6). Some interesting features are immediately apparent in the low-resistivity cases. Just as with the 135° clock angle case, we now have multiple nulls appearing. We also find FTEs occurring regularly in the cusps where the currents are most intense. The figure shows one such flux rope (see black magnetic field lines) in the Southern Hemisphere. The physical origins of the multiple nulls that appear in the low-resistivity case are unknown and an active area of research that we do not attempt

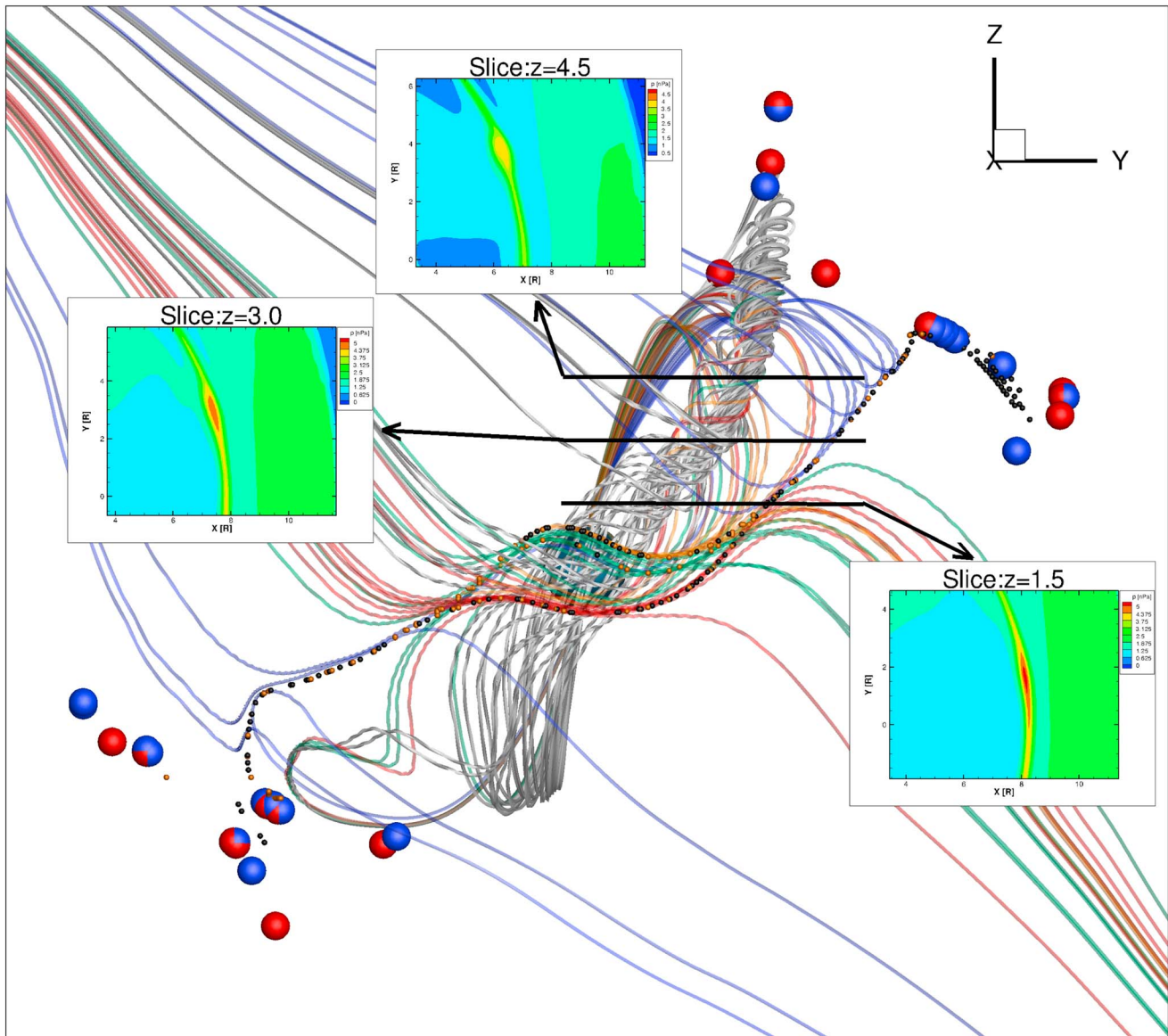


Figure 9. A view from the Sun to Earth of the FTE in relation to the separator points. The field lines associated with the FTE are in grey, field lines near the lower branch of the separator are in red, middle branch in green, and upper branch in orange. Blue lines are field lines near the regions before the separator branches. Also show are cut planes through the FTE showing the characteristic pressure bulge associated with the FTE.

to address in the present study. We note that in a given hemisphere the number of all new positive and negative nulls (that add up to the classical single null) is the same. Perhaps, most intriguing is the presence of multiple, clearly distinguished, magnetic separators on the dayside magnetopause. These separators do not quite reach the nulls due to a restricted search domain and not due to a rendering problem or limitation of the algorithm. It is not immediately obvious which of these separators is controlling the production of open magnetic flux. We therefore integrate the parallel electric field along each of these seven separators to see if one has a dominant contribution to open flux production. That integral is equivalent to within a few percent regardless of which separator is chosen indicating that any separator can be chosen. The reason is that each of the separators is separating islands of magnetic flux. Since each island must balance the open flux produced by its neighbor, the integrated parallel electric field must be equivalent in all cases. As to the physical origin of the multiple separators, we can only speculate at this point. We believe that the current sheet thins as the resistivity decreases to the point where the current sheet becomes unstable. As the instability ensues, the separatrix surfaces, which are already very close together for much of the magnetopause, come into contact to form additional separators.

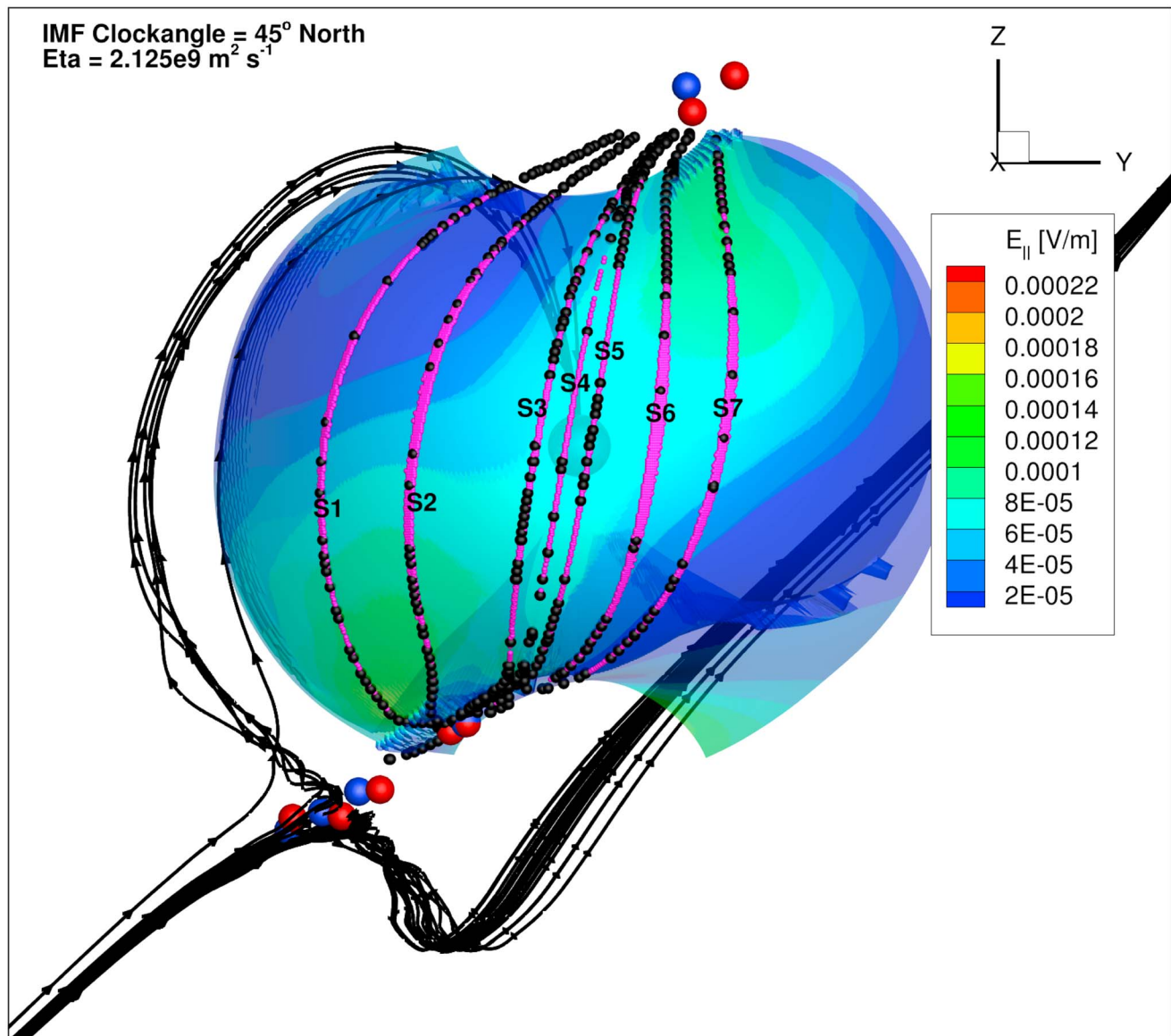


Figure 10. We use method 1 (pink dots) and method 3 (black dots) to calculate magnetic separators for a low η case when the solar wind clock angle is 45° northward. Note that seven distinct separator are found on the dayside as are multiple nulls in the cusp. FTEs are also seen to periodically form at high latitudes near the cusps (see black field lines).

There is an interesting question of physical and topological stability in the formation of multiple separators in the low-resistivity cases. In both clock angle cases, there is clearly an instability going on that results in the generation of multiple separators. At this time, we are unable to ascertain if these instabilities are physical or topological in nature. Such analysis is therefore left to future studies.

4. Discussion and Conclusions

In this paper we introduce three methods for finding magnetic separators in global magnetospheric simulations. All three methods are demonstrated to give the same results. Methods 1 and 3 do not involve finding nulls and are both easy to parallelize in an “embarrassingly parallel” manner which enables finding the separator to high accuracy relatively rapidly using readily available supercomputing resources. In applying the method to the dayside magnetopause, we are able to draw a number of interesting conclusions which we focus on in this section.

For the large-resistivity case and predominately northward IMF, E_{\parallel} maximizes at the subsolar point, not in the cusp. Therefore, the main contribution to the reconnection rate as measured by the contribution to the open flux production is also at the subsolar point. This picture is in contrast to the 2-D picture put forth by *Dungey* [1961]. However, the result is consistent with the study of *Dorelli et al.* [2007] which also attempted to find separators under predominantly northward IMF conditions using the OpenGGCM code.

The low-resistivity version of the predominantly northward IMF case shows the formation of multiple separators and FTEs forming near the cusp. For the separator near the subsolar point E_{\parallel} maximizes near the subsolar point, while the separators farthest from the subsolar point show E_{\parallel} maximizing in the cusp. FTEs are seen in the cusps in observational studies [e.g., *Sibeck et al.*, 2005], and at least one other simulation study [*Berchem et al.*, 1995]. We believe that a low resistivity, combined with uniformly resolving the dayside magnetopause such that both low and high latitudes have the same high resolution and low numerical contribution to the resistivity, allows the current sheet at high latitude to thin and become unstable resulting in the FTE formation.

The separator calculation under northward IMF has some interesting implications for the “antiparallel/component” reconnection debate. Reconnection on the magnetopause is often thought of in terms of component reconnection or antiparallel reconnection. These views of how reconnection occurs at the magnetopause are derived from two-dimensional theory of magnetic reconnection. Component reconnection is essentially a generalization of 2-D reconnection in the presence of a guide field [*Sonnerup*, 1974]. In contrast, antiparallel reconnection in the context of the magnetopause argues that reconnection occurs where the IMF and magnetospheric magnetic fields are most antiparallel [*Crooker*, 1979; *Tsyganenko and Stern*, 1996]. The antiparallel picture is consistent with the idea that reconnection is a local process associated with the magnetic nulls in the 2-D picture of *Dungey* [1961]. There exists supporting evidence for each of these paradigms. Observations of reconnection equatorward of the cusp for northward IMF [see e.g., *Fuselier et al.*, 1997] support the view of component reconnection, but signatures of plasma acceleration across rotational discontinuities [see e.g., *Cowley*, 1982] support the antiparallel view.

In contrast, we find that reconnection is happening at all points along the separator, in both low- and high-resistivity cases. This result is consistent with earlier results by *Dorelli et al.* [2007] and *Parnell et al.* [2010]. Therefore, the interpretation of antiparallel reconnection occurring near the cusps and component reconnection occurring near the subsolar point are really just local views of the 3-D global separator(s). Separator reconnection thus provides a unifying picture for these two disparate perspectives. In other words, both antiparallel and component reconnection are occurring, which is observed depends on which part of the separator you are on.

Examining separator reconnection during FTE formation under predominantly southward IMF yields the fascinating demonstration that open flux production decreases locally during FTE formation. The local electric field decrease for the case examined is approximately 25% resulting in a decrease of the global reconnection rate of approximately 4%. This is in contrast to the picture that many people have of FTEs being indicative of active reconnection, and the lack of FTEs meaning that reconnection is “quenched” [*Haerendel et al.*, 1978; *Russell and Elphic*, 1979]. Moreover, our analysis during FTE formation demonstrates that the magnetic topology, as measured by the number of separators, becomes more complex; three distinct branches of the separator are found in the vicinity of the FTE. The two-dimensional picture holds that there are two x points and an o point, whereas the three-dimensional picture is more complete and shows that there are only topological X lines. These findings are consistent with the work of *Dorelli and Bhattacharjee* [2009] which demonstrate that FTEs form spontaneously without dipole tilt and that multiple separators should be present during the formation; our study traces those branches and evaluates the consequences on the global reconnection rate.

In our simulation setup, we do our best to reduce any potential physical source of asymmetry. The final results for the low-resistivity case, however, does exhibit an asymmetric magnetosphere. We speculate origin of the asymmetry relates to asymmetry in the perturbation that triggers current-driven instability on the magnetopause. In the low-resistivity case, the current sheet thins to the point of instability. At that point there must be a perturbation that triggers the instability and for asymmetry to form that perturbation must be asymmetric. Presumably, the seed for the instability comes from some combination of roundoff error, slightly different accumulated numerical error in the solar wind propagation, or slightly different triggering of the slope limiter in the numerical scheme. Roundoff errors in particular are random and asymmetric, and the asymmetric differences can grow exponentially if the system is unstable. This is the usual path to symmetry breaking in

numerical codes. It is also conceivable that a numerical issue exists whose timescale is long enough to be damped by sufficiently large resistive terms. Given the extensive verification of numerical schemes implemented in BATS-R-US with standard MHD test problems, we regard this last possibility is unlikely. Nevertheless, the exact source of the initial perturbation is unknown. However, such behavior is regularly seen in global MHD simulations. Moreover, the real magnetosphere should be expected to have asymmetric perturbations. Therefore, we believe these results are still applicable to the problem at hand.

There are some caveats to applying the above results too broadly. Most obviously is the fact that our simulations are using resistive MHD with a uniform resistivity. The results may be different if we were to employ a different resistivity model, but we do not explore that dependence in this study. Likewise, numerical resistivity could possibly play a role in the low η results. Our grid is chosen to minimize this impact, but it is difficult to quantify just how much effect numerics has on the result.

The algorithms demonstrated here are not specific to any particular implementation of a global magnetosphere code. These same algorithms are equally applicable to any of the global MHD codes in the community, not just the BATS-R-US model that we used for demonstration. They are even applicable to non-MHD type codes as the algorithms only depends on being able to identify topology.

Acknowledgments

Resources supporting this work were provided by the NASA High-End Computing (HEC) Program through the NASA Advanced Supercomputing (NAS) Division at Ames Research Center and the NASA Center for Climate Simulation (NCCS) at Goddard Space Flight Center. A. Glocer effort was supported by a project through the NASA Living With A Star program and J. Dorrelli was supported by a NASA Geospace SR&T project. P.A. Cassak was supported by NSF grant AGS-0953463. The tool used to locate separators will be made available through the Community Coordinated Modeling Center (CCMC), and the BATS-R-US code used to run the numerical simulations is available through the University of Michigan for download.

References

- Berchem, J., J. Raeder, and M. Ashour-Abdalla (1995), Reconnection at the magnetospheric boundary: Results from global magnetohydrodynamic simulations, in *Physics of the Magnetopause*, edited by P. Song, B. Sonnerup, and M. Thomsen, pp. 205–213, AGU, Washington, D. C.
- Beveridge, C. (2006), A new method for finding topological separators in a magnetic field, *Sol. Phys.*, 236(1), 41–57, doi:10.1007/s11207-006-0124-3.
- Boozer, A. H. (2005), Physics of magnetically confined plasmas, *Rev. Mod. Phys.*, 76, 1071–1141, doi:10.1103/RevModPhys.76.1071.
- Close, R., C. Parnell, and E. Priest (2004), Separators in 3D quiet-sun magnetic fields, *Sol. Phys.*, 225(1), 21–46, doi:10.1007/s11207-004-3259-0.
- Cowley, S. W. H. (1973), A qualitative study of the reconnection between the Earth's magnetic field and an interplanetary field of arbitrary orientation, *Radio Sci.*, 8, 903–913, doi:10.1029/RS008i011p0903.
- Cowley, S. W. H. (1982), The causes of convection in the Earth's magnetosphere—A review of developments during the IMS, *Rev. Geophys.*, 20, 531–565, doi:10.1029/RG020i003p00531.
- Crooker, N. (1979), Dayside merging and cusp geometry, *J. Geophys. Res.*, 84, 951–959.
- Dorelli, J. C., A. Bhattacharjee, and J. Raeder (2007), Separator reconnection at Earth's dayside magnetopause under generic northward interplanetary magnetic field conditions, *J. Geophys. Res.*, 112, A02202, doi:10.1029/2006JA011877.
- Dorelli, J. C., and A. Bhattacharjee (2009), On the generation and topology of flux transfer events, *J. Geophys. Res.*, 114, A06213, doi:10.1029/2008JA013410.
- Dungey, J. (1961), Interplanetary magnetic field and the auroral zones, *Phys. Rev. Lett.*, 93, 47–48.
- Fuselier, S. A., B. J. Anderson, and T. G. Onsager (1997), Electron and ion signatures of field line topology at the low-shear magnetopause, *J. Geophys. Res.*, 102, 4847–4864, doi:10.1029/96JA03635.
- Glocer, A., G. Toth, T. Gombosi, and D. Welling (2009a), Modeling ionospheric outflows and their impact on the magnetosphere, initial results, *J. Geophys. Res.*, 114, A05216, doi:10.1029/2009JA014053.
- Glocer, A., G. Toth, Y. Ma, T. Gombosi, J.-C. Zhang, and L. M. Kistler (2009b), Multifluid Block-Adaptive-Tree Solar wind Roe-type Upwind Scheme: Magnetospheric composition and dynamics during geomagnetic storms—Initial results, *J. Geophys. Res.*, 114, A12203, doi:10.1029/2009JA014418.
- Glocer, A., G. Toth, M. Fok, T. Gombosi, and M. Liemohn (2009), Integration of the radiation belt environment model into the space weather modeling framework, *J. Atmos. Sol. Terr. Phys.*, 71, 1653–1663, doi:10.1016/j.jastp.2009.01.003.
- Gombosi, T. I., G. Toth, D. L. De Zeeuw, K. C. Hansen, K. Kabin, and K. G. Powell (2001), Semi-relativistic magnetohydrodynamics and physics-based convergence acceleration, *J. Comput. Phys.*, 177, 176–205.
- Greene, J. M. (1988), Geometrical properties of three-dimensional reconnecting magnetic fields with nulls, *J. Geophys. Res.*, 93, 8583–8590, doi:10.1029/JA093iA08p08583.
- Haerendel, G., G. Paschmann, N. Sckopke, and H. Rosenbauer (1978), The frontside boundary layer of the magnetosphere and the problem of reconnection, *J. Geophys. Res.*, 83, 3195–3216, doi:10.1029/JA083iA07p03195.
- Haynes, A., and C. Parnell (2010), A method for finding three-dimensional magnetic skeletons, *Phys. Plasmas*, 17, 92,903, doi:10.1063/1.3467499.
- Hesse, M., and K. Schindler (1988), A theoretical foundation of general magnetic reconnection, *J. Geophys. Res.*, 93(A6), 5559–5567, doi:10.1029/JA093iA06p05559.
- Komar, C. M., P. A. Cassak, J. C. Dorelli, A. Glocer, and M. M. Kuznetsova (2013), Tracing magnetic separators and their dependence on IMF clock angle in global magnetospheric simulations, *J. Geophys. Res. Space Physics*, 118, 4998–5007, doi:10.1002/jgra.50479.
- Laitinen, T. V., P. Janhunen, T. I. Pulkkinen, M. Palmroth, and H. E. J. Koskinen (2006), On the characterization of magnetic reconnection in global MHD simulations, *Ann. Geophys.*, 24, 3059–3069, doi:10.5194/angeo-24-3059-2006.
- Laitinen, T. V., M. Palmroth, T. I. Pulkkinen, P. Janhunen, and H. E. J. Koskinen (2007), Continuous reconnection line and pressure-dependent energy conversion on the magnetopause in a global MHD model, *J. Geophys. Res.*, 112, A11201, doi:10.1029/2007JA012352.
- Lau, Y.-T., and J. M. Finn (1990), Three-dimensional kinematic reconnection in the presence of field nulls and closed field lines, *Astrophys. J.*, 350, 672–691, doi:10.1086/168419.
- Longcope, D. (1996), Topology and current ribbons: A model for current, reconnection and flaring in a complex, evolving corona, *Sol. Phys.*, 169(1), 91–121, doi:10.1007/BF00153836.
- Parnell, C. E., A. L. Haynes, and K. Galsgaard (2010), Structure of magnetic separators and separator reconnection, *J. Geophys. Res.*, 115, A02102, doi:10.1029/2009JA014557.

- Priest, E. R., and T. G. Forbes (2000), *Magnetic Reconnection: MHD Theory and Applications*, Cambridge Univ. Press, Cambridge, U. K.
- Russell, C. T., and R. C. Elphic (1979), ISEE observations of flux transfer events at the dayside magnetopause, *Geophys. Res. Lett.*, *6*, 33–36, doi:10.1029/GL006i001p00033.
- Schindler, K., and M. Hesse (1988), General magnetic reconnection, parallel electric fields and helicity, *J. Geophys. Res.*, *93*, 5547–5557.
- Sibeck, D. G., G. I. Korotova, V. Petrov, V. Styazhkin, and T. J. Rosenberg (2005), Flux transfer events on the high-latitude magnetopause: Interball-1 observations, *Ann. Geophys.*, *23*, 3549–3559, doi:10.5194/angeo-23-3549-2005.
- Sonnerup, B. (1974), Magnetopause reconnection rate, *J. Geophys. Res.*, *79*, 1546.
- Titov, V. S., Z. Mikic, T. Török, J. A. Linker, and O. Panasenco (2012), 2010 August 1–2 sympathetic eruptions. I. Magnetic topology of the source-surface background field, *Astrophys. J.*, *759*(1), 70, doi:10.1088/0004-637X/759/1/70.
- Tóth, G., Y. J. Ma, and T. I. Gombosi (2008), Hall magnetohydrodynamics on block adaptive grids, *J. Comput. Phys.*, *227*, 6967–6984, doi:10.1016/j.jcp.2008.04.010.
- Tsyganenko, N. A., and D. Stern (1996), Modeling the global magnetic field of the large-scale Birkeland current systems, *J. Geophys. Res.*, *101*, 27,187–27,198.
- Vasyliunas, V. (1975), Theoretical models of magnetic field line merging, *Rev. Geophys.*, *13*(1), 303–336.